

# 2D Tomographic Maps of Rayleigh and Love Waves for Armenia and Its Surrounding Areas

Seyed Hossein Abrehdari\*,1,2,3, Jon K. Karapetyan<sup>1</sup>, Habib Rahimi<sup>2</sup>, and Eduard Geodakyan<sup>1</sup>

Abstract: This study aims to provide 2D tomography images of surface wave group velocity in Armenia and its neighboring regions within the Eurasian-Arabic plates, aiming to enhance the understanding of the shear velocity structure in the area. In this context,  $\sim 516$  earthquakes ( $M \ge 3.5$ ) recorded by 20 stations between 1999-2018 were analyzed, and the surface wave group velocity dispersion curves for each record (source-station path) were estimated. Subsequently, taking advantage of a 2D-linear inversion procedure, 2D tomography maps for periods of 5–80 s (Depth  $\approx 180$  km) were computed with a grid spacing of  $0.2^{\circ} \times 0.5^{\circ}$ . The results of this research indicate that short-periods  $(5 \le T \le 25 \text{ s})$  are more influenced by shallow, ever-evolving deformations within various geological units, such as sedimentary basins. A minor low-velocity anomaly (Depth ≈ 27 km) is observed on the northwest slope of the Aragats volcano, which contrasts with the findings of earlier studies. For Rayleigh and Love waves, the North Armenia Block is covered by a high-velocity anomaly. The results for medium periods reveal the presence of very-high-velocity anomalies in some geological units (e.g., Lesser Caucasus), aligning with the ongoing subduction processes. In contrast, very lowvelocity anomalies reflect the uppermost mantle information, revealing an extremely thin lithosphere accompanied with a hot asthenosphere. The findings for long-periods of Love and Rayleigh waves in Armenia reveal an almost uniform velocity distribution pattern, along with very-low-velocity anomalies in the uppermost mantle, attributed to a thin lithosphere or the lack of lithospheric mantle in most units of the study region. The results demonstrate an acceptable accordance with known geological features in the Eurasian-Arabic ongoing collision zone. Overall, the main strengths of this paper lie in the application of a tomographic technique utilizing an important data set. The findings have the potential to provide new insights into the Armenian region and its surrounding areas.

**Keywords:** Republic of Armenia, 2D Rayleigh and Love surface wave tomography, Dispersion curve, Group velocity.

Citation: Abrehdari, S. H., J. K. Karapetyan, H. Rahimi, and E Geodakyan (2025), 2D Tomographic Maps of Rayleigh and Love Waves for Armenia and Its Surrounding Areas, *Russian Journal of Earth Sciences*, 25, ES3014, EDN: SBYWRB, https://doi.org/10.2205/2025es001019

#### RESEARCH ARTICLE

Received: February 3, 2025 Accepted: May 6, 2025 Published: June 19, 2025



Copyright: © 2025. The Authors. This article is an open access article distributed under the terms and conditions of the Creative Commons Attribution (CC BY) license (https://creativecommons.org/licenses/by/4.0/).

## 1. Introduction

The Greater Caucasus and Lesser Caucasus are separated by the Transcaucasian (Dzirula) Massif, the Kura, and Rioni rivers flowing between them. The convergence of the Arabian and Eurasian plates began during the Late Cretaceous period. This movement gradually resulted in a series of intensive collisions between the Arabian plate and the smaller continental blocks that emerged from the break-up of Gondwana until the final closure of Neotethys Ocean [Golonka, 2004]. This continent-continent collision has intensified the main seismoactive structures in NW Iran, the Greater Caucasus (GC), the Lesser Caucasus (LC), and Eastern Anatolia (EA), specified by compressional features such as thrusts, nappes, reverse faults, and highly deformed fault-propagation folds [DeMets et al., 1990].

<sup>&</sup>lt;sup>1</sup>Institute of Geophysics and Engineering Seismology, National Academy of Sciences, Gyumri, Armenia

<sup>&</sup>lt;sup>2</sup>Institute of Geophysics, University of Tehran, Tehran, Iran

<sup>&</sup>lt;sup>3</sup>Institute of Seismology, University of Helsinki, Helsinki, Finland

<sup>\*</sup> Correspondence to: Seyed Hossein Abrehdari, abrehdari@ut.ac.ir

Geologically, the Republic of Armenia is a landlocked country located on the slopes of the Lesser Caucasus, at the convergence of multiple micro-plates, island arcs, and active margins characterized by collision, subduction, and accretion processes. This region lies between the Black Sea and the Caspian Sea, which are relicts of the Tethys paleo-oceanic systems. In Armenia, the geological evolution of the Yerevan-Ordubad synclinorium reflects its history as a geoanticline during the Jurassic period. This structure underwent significant subsidence in the Paleogene period, followed by a phase of substantial uplift in the Miocene period [Kornev, 1963].

The intrusive magmatism in Armenia can be categorized into two distinct stages: during the upper Cretaceous period, significant magma products were introduced into intrusive rifts, resulting in the formation of ultrabasite masses. Following that, granitoid intrusions formed during the Paleogene-Neogene period. This geological progression is clearly illustrated on the Map of the Deep Structure of the Caucasus based on satellite data [Eppelbaum and Khesin, 2012].

It is important to highlight that the Central Armenia Block (CAB) has been built from the complex landscape of the region, and the presence of numerous intrusive faults indicates a high level of tectonic activity. The sedimentary deposits in this area are relatively thickness, with the Quaternary sedimentary layer above the Paleozoic metamorphic foundation being particularly shallow. This situation suggests a significant risk of earthquakes and the potential for extensive destruction that may follow. The low thickness of the deposits once more indicates to the presence of orogenic regime and erosion in the region, very active erosion, closeness of the metamorphic foundation to the surface, while the location of blocks in the area subject to pressures denotes the high geodynamic activity at this territory [Eppelbaum and Khesin, 2012].

This interaction has led to the formation of transform faults in northern and eastern Anatolia, where various microplates slide past each other at relatively high speeds, resulting in the creation of stripes. Consequently, the pressing and pulling segments had emerged; subduction, sliding had occurred, and from the edges of the bordering massifs, snaps (in the form of spanning massifs) had come about [*Trifonov and Makarov*, 1988].

The Menderes, Artvin-Bolnisi, and Alagoz-Julfa tectonic units, which are thought to be components of the greater Central Iran tectonic unit, played a significant role in geological formation of the region. During the Oligocene-Miocene epoch, the Central Iran massif was fragmented into distinct uplifts and troughs, leading to the formation of the Middle Aras depression zone [Echle, 1974]. The North Anatolian Fault, extending to Erzurum, branches into two paths: one traverses the Kars volcanic plateau and continues into Armenia, while the other ascends along the upper reaches of the Aras River. The last branch is divided into the Arazyani and Nakhchivan faults, which delineate the Middle Aras depression zone. These faults are connected to the North Anatolia Fault and active as part of a transform fault system, and resemble each other in many aspects of geological features. The previously mentioned faults, along with others, suggest that the geological structure of the Yerevan and Nakhchivan regions is composed of blocks, which has led to the development of numerous horst-anticlinal and graben-synclinal tectonic features, as well as the accumulation of Oligocene-Quaternary sedimentary deposits. Positioned perpendicular to the Aras River, the "island" uplifts (such as Ararat) were divided into small lowlands [Gurbanov et al., 2024] (Figure A2).

The relatively high pressure exerted by the smaller plates of the large Arabian-Eurasian and Central Iranian plates, combined with pulling and deformation movements, has led to the formation of thrust faults and complex tectonic structure, exaggerating its geotectonic activity.

Intensive ground volcanic processes took place till the anthropogenic period. Lava layers had covered not only east of Anatolia, but also central and southern parts of Lesser Caucasus and Iran. The Lesser Caucasus system including Bazum, Pambak-Sevan, Zangazur, Vardenis, and Gegham mountain ranges surround most of the Armenia located in the Transcaucasian volcanic plateau.

A lowland exists between the Gegham and Sevan mountains. Aragats is the largest volcanic massif in the South Caucasus, with its highest peak being the Northern Summit at 4090 m. Other notable summits include Kaputjugh (3904 m), Vardenis (3522 m), and Ajdaak (3597 m). To the northwest of Armenia lies the Shirak Plain, while the southwest features the Ararat Plain. The average elevation of the region is 900 m, with over 90% of Armenia situated above 1000 m and an overall average height of 1800 m. The lowest areas are found in the basins of the Debed and Aras Rivers, at around 380 m. The lowlands are relatively small in size. Most settlements in the basins of the Vorotan, Vokhchi, and Aras Rivers are located on slopes of 30 degrees, which complicates urban transportation organization and development.

Comprehensive geophysical studies have been carried out in the Caucasus utilizing seismic reflection and refraction techniques [e.g., Adamiya et al., 1992; Eppelbaum and Khesin, 2012; Ismail-Zadeh et al., 2020] as well as body wave tomography methods [e.g., Koulakov et al., 2012; Legendre et al., 2017; Raykova and Nikolova, 2007; Skobeltsyn et al., 2014; Zabelina et al., 2016]. Notably, most of these investigations focused on analyzing body waves at both large and small scales to assess the crustal thickness beneath the region.

Some surface wave tomography studies have been undertaken [e.g., *Huang et al.*, 2003; *Ritzwoller and Levshin*, 1998], primarily focusing on the mainland Caucasus scale, with only a few studies of surface waves specifically in Armenia. The relatively limited earthquake data, sparse seismic stations, and reliance on teleseismic earthquakes highlight the need for similar studies that utilize a high-quality database to be conducted and repeated.

Perkins tomography study [Perkins, 2019] reveals that seismic waves travel more rapidly through cold-rigid materials (like a subduction plate inside the mantle) and more slowly through hotter materials (like rising hot rocks). Since surface waves have significantly higher amplitudes than body waves and primarily sample the Earth's near-surface rather than its deeper layers, they are valuable tools for geotechnical surveys. Therefore, this research utilizes surface waves to generate and analyze high-resolution 2D tomography maps of geological structures based on their dispersion curves.

In recent years, the deployment of broadband seismic stations in the Caucasus region has enhanced path coverage, leading to improved tomographic imaging of the area [Legendre et al., 2017; Tseng et al., 2016]. In this research, the utilized seismic data were from the Incorporated Research Institutions for Seismology (IRIS) including Armenia, Turkey, Azerbaijan, and Armenian Seismological Network (ARMNET); NW Iran – Iranian Seismological Center (IRSC), and Iranian National Broadband Seismic Network (INSN). This array features an adequate density and non-uniform distribution of stations throughout the network, along with excellent spatial and azimuthal coverage resulting from the interstation paths. This configuration provides a nearly ideal array for the application of tomography.

In this study, Rayleigh wave group velocity dispersion curves were calculated for each source-station path using the single-station method with Herrmann's do\_mft package [Herrmann, 2013]. Then, 2D group velocity maps were created through a 2D linear inversion technique developed by [Ditmar and Yanovskaya, 1987; Yanovskaya and Ditmar, 1990].

In this context, data from local-regional earthquakes recorded by 21 broadband stations (refer to Table A1) were employed. The tomography map results are presented for a period of 5–80 s. The study's findings for short-periods indicate distinct velocity anomalies in basins, along faults, and beneath volcanic uplifts. In contrast, the velocity maps for medium and long periods display reveal ultra-fast (dark blue shades) and ultra-slow (dark red shades) velocity anomalies across different geological units in the Caucasus.

This study benefits a rich earthquake database spanning from 1999–2023, along with new permanent seismic stations within the mentioned array (IRIS, IRSC, INSN, and ARMNET). This combination significantly enhances ray path coverage in the Caucasus, leading to improved resolution of tomography velocity maps. This study also employs a checkerboard test as described by [*Yanovskaya et al.*, 1998]. In this test, computer scripts were employed to account for not only a uniform distribution of ray paths but also various effective parameters, such as basic earthquake data parameters,  $\sigma$ ,  $\alpha$ , uniform dispersion, optimal data density distribution, averaging area (L), and stretching ( $\varepsilon$ ).

The main goal of this research is to create 2D tomographic maps by leveraging the scattering characteristics of surface Rayleigh and Love waves in Armenia in order to better understand the velocity structure associated with tectonic interactions, concentrating on the fluctuations in velocity anomalies (both increases and decreases) from the upper mantle to the crust over periods 5–80 s. For this purpose, specialized codes were executed in MATLAB and GMT (Generic Mapping Tools software) [Wessel and Smith, 1995], and by observing the results for various solutions, the 2D tomography images were plotted (Figures 5 and 6). The plotted maps exhibit a proper correlation with the well-known geological and tectonic features of the Caucasus.

This research examined several prior tomography studies [e.g., *Koulakov et al.*, 2012; *Legendre et al.*, 2017; *Zabelina et al.*, 2016] and made slight modifications to the measurement techniques and inversion method for the observations by employing specialized computer scripts. Furthermore, it increased the number of stations outfitted with new sensors, as well as the variety of events and the extent of route coverage within the study area compared to earlier research. Nonetheless, enhancing the density of data and stations for future studies will aid in the interpretation of finer-scale velocity structures. It is important to emphasize that the current coverage is still inadequate.

### 2. Data and study area

#### 2.1. Study area

The primary emphasis of this study is on Armenia, although variations in velocity anomalies in the surrounding regions are also taken into account. For this purpose, Armenia was divided into three distinct blocks: The Northern Armenia Block (NAB), which includes the Shirak, Lori, and Tavush provinces; the Central Armenia Block (CAB), encompassing the Gegharkunik, Ararat, Kotayk, Aragatsotn, Armavir, and Yerevan provinces; and the Southern Armenia Block (SAB), comprising the Vayots Dzor and Syunik provinces. The labeled geological units used for interpreting the 2D tomography maps of the study area are depicted in Figure 1a.

The study area, which is Armenia, along with the locations of earthquake epicenters, path coverage, and the histogram of ray distribution corresponding to the periods utilized in this research, are presented in Figure 1a–1d.

#### 2.2. Data

In this study, recorded local-regional earthquake data were used with magnitude  $M \ge 3.5$  that occurred in the Armenia and its surrounding regions with geographic coordinates (43°–47.5°E and 38°–41.5°N; Depth  $\approx 180$  km), during the period 1999–2023. A total of 516 high quality events, recorded by the 21 three-component broadband digital stations installed in mentioned array (IRIS, IRSC, INSN, and IASBS) was selected, which provides much better ray path coverage in Armenia.

The seismic network consists of broadband seismometers (Guralp CMG-3T/CMG-40T) for IRIS GSN with recording data with 24 bits of resolution in continuous time series with at least a 20 samples per second (sps) sampling rate. For IRSC broadband instruments (e.g., CMG-3T) 24-bit digitizers which manufactured by Guralp and Nanometrics company, respectively. IRSC stations operate in continuous mode with a sampling rate of 50 samples per second (sps). The new established seismic network in Armenia (Armenian Seismological Network – ARMNET) includes 8 new borehole broadband sensors. The Garni (GNI) station is equipped with a Data Logger Q330-HR and Streckeisen STS-1VBB w/E300 Trillium 240 broadband seismometer. In addition, the Iranian National Seismological Center (INSN) consists of broadband CMG-3T seismometers that have 24-bit recorders (sampling rate of 50 sps) produced by Guralp company.

A total of nearly 49,000 vertical and transverse components of local and regional waveform data from surface-wave seismograms were gathered for processing. This includes  $\sim$  27,000 components for Rayleigh waves and  $\sim$  22,000 for Love waves, sourced from the mentioned stations.

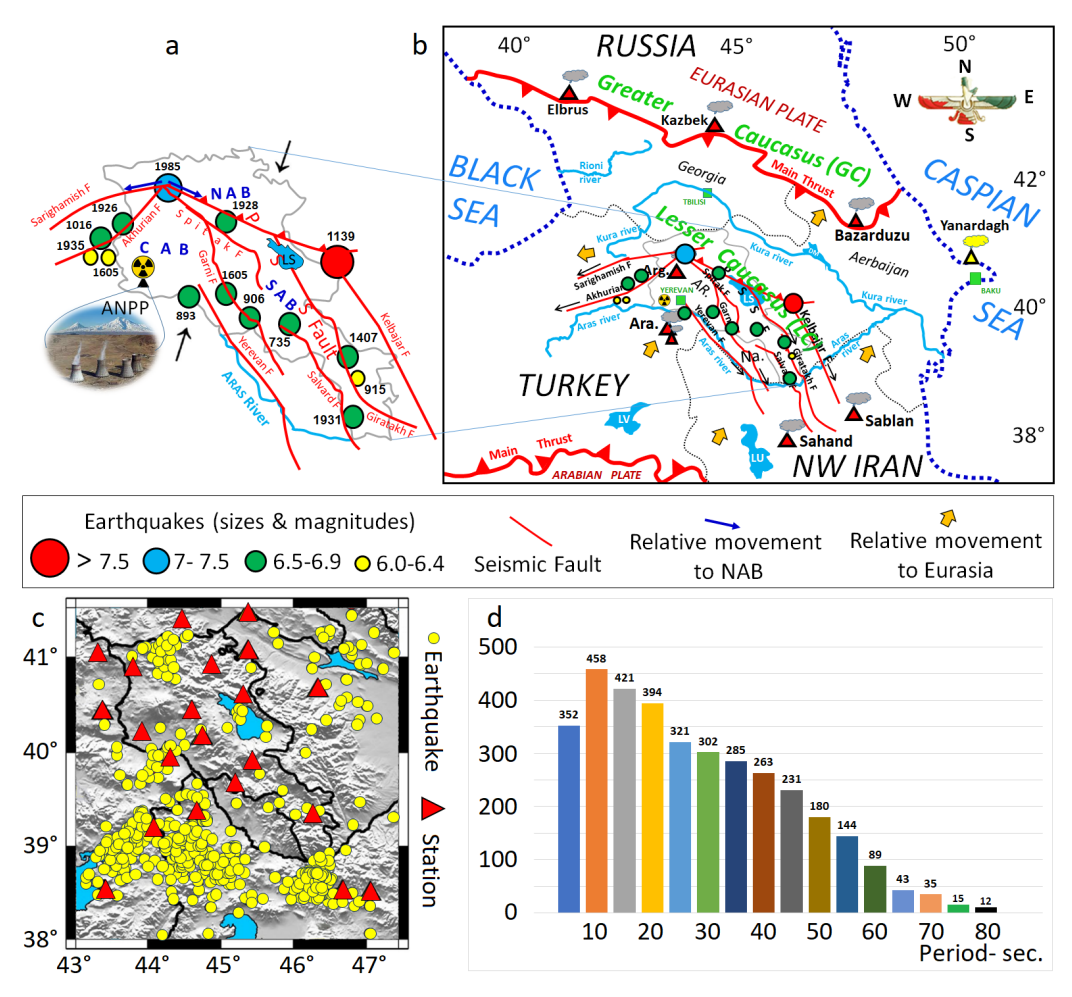


**Figure 1.** a. The study area (Armenia) and active faults and epicenter of major historic earthquakes in and around Armenia [Karakhanian et al., 2004]; b. The different geological units of Caucasus. Retrieved from [Irbashyan et al., 2001; Khuduzade and Jafarov, 2017]; c. Geographical distribution of the 20 seismic stations (red triangles) and of the epicenters (yellow circles) of the 516 earthquakes considered in this study, on shaded topography map; d. The number of paths utilized in the tomography inversion compared to the period in this study. Abbreviations: Ar. – Armenia, Arg. – Aragats, Ara. – Ararat, ANPP – Armenian Nuclear Power Plant, LS – Lake Sevan, PSSF – Pambak-Sevan-Syunik Fault, NAB – Northern Armenia block, CAB – Central Armenia block, and SAB – Southern Armenia block (with slightly modifications by Abrehdari).

## 3. Resolution of tomography images

Before interpreting the derived seismic model, we must first conduct several tests to evaluate the robustness of the solution. Traditionally, spatial resolution in seismic tomography is assessed through checkerboard tests, which involve reconstructing periodically defined synthetic anomalies. One approach to assess the quality of data and evaluate its ability to reconstruct velocity structures is to generate synthetic data with similar characteristics to real data. In this method, a velocity model of the Earth is considered, and the radiation velocity is derived from the synthetic model using the radiation coverage in the actual data. Then, the synthetic data is entered into the inversion process to check the recovery rate of the original model.

First, the study area was gridded into  $0.2^{\circ} \times 0.5^{\circ}$  blocks (Figure 2a). To determine the accuracy and separability of the final model at different periods (T=5-75 s), the checkerboard test was tested along with Gaussian random error ( $0.1 \, \text{km/s}$ ). The degree of accuracy and separability is influenced by the path coverage. Figure 2 illustrates the effective recovery rate of the model inside the study area for odd periods ranging from 5

to 75 s. However, some segments of the region (particularly at the margins) and longer periods (T = 55, 65, and 75 s) show stretching of the blocks due to insufficient ray coverage. For more details, refer to [*Abrehdari et al.*, 2022, 2023].

In the 2D tomography method developed by [ $Yanovskaya\ et\ al.$ , 1998], a parameter known as the averaging area (L) is provided, which enables the measurement of data separation power (Figure 2).

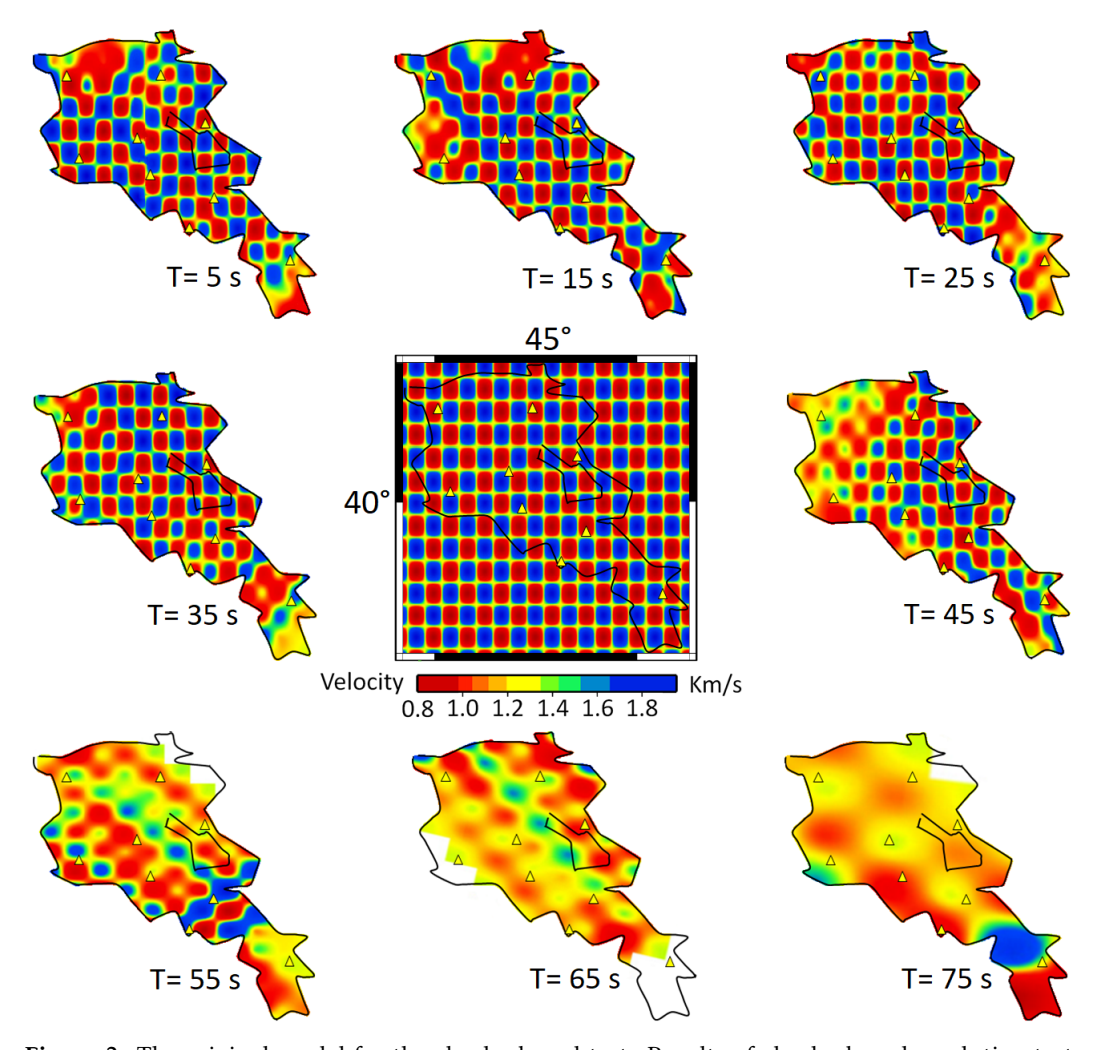


**Figure 2.** The original model for the checkerboard test. Results of checkerboard resolution test for odd periods ranging from 5–75 s. In this test, a Gaussian noise error with a mean of zero and a standard deviation of 0.1 km/s has been added to the observations. Some white (T = 55, 65, and 75 s) segments of the region (particularly at the margins) and longer periods show stretching of the blocks (shades) due to the lack of proper beam coverage.

In the checkerboard test method, the optimal values for the averaging area (L) and stretching ( $\varepsilon$ ) are established not only by ensuring a uniform distribution of ray paths but also by utilizing computer scripts that incorporate various effective parameters, including basic earthquake parameters,  $\sigma$ ,  $\alpha$ , uniform dispersion, and optimal data density distribution. For more details on the variations in the  $\sigma$  and  $\alpha$  parameters, refer to Figures 2 and 3, as well as [*Abrehdari et al.*, 2023].

The arrangement of regular and dense geometric arrays of seismic stations, along with the distribution of numerous ray paths, influences the resolution and accuracy of tomographic images. This results in enhancements to parameters such as the averaging area (L) and stretching ( $\varepsilon$ ). Figure 3 illustrates how the number of paths, stations, earthquakes, and resolution parameters such as  $\varepsilon$  and L change with varying periods and depths. Yanovskaya [Yanovskaya, 1997] introduced the concept of averaging area (L) in order to parameterize the

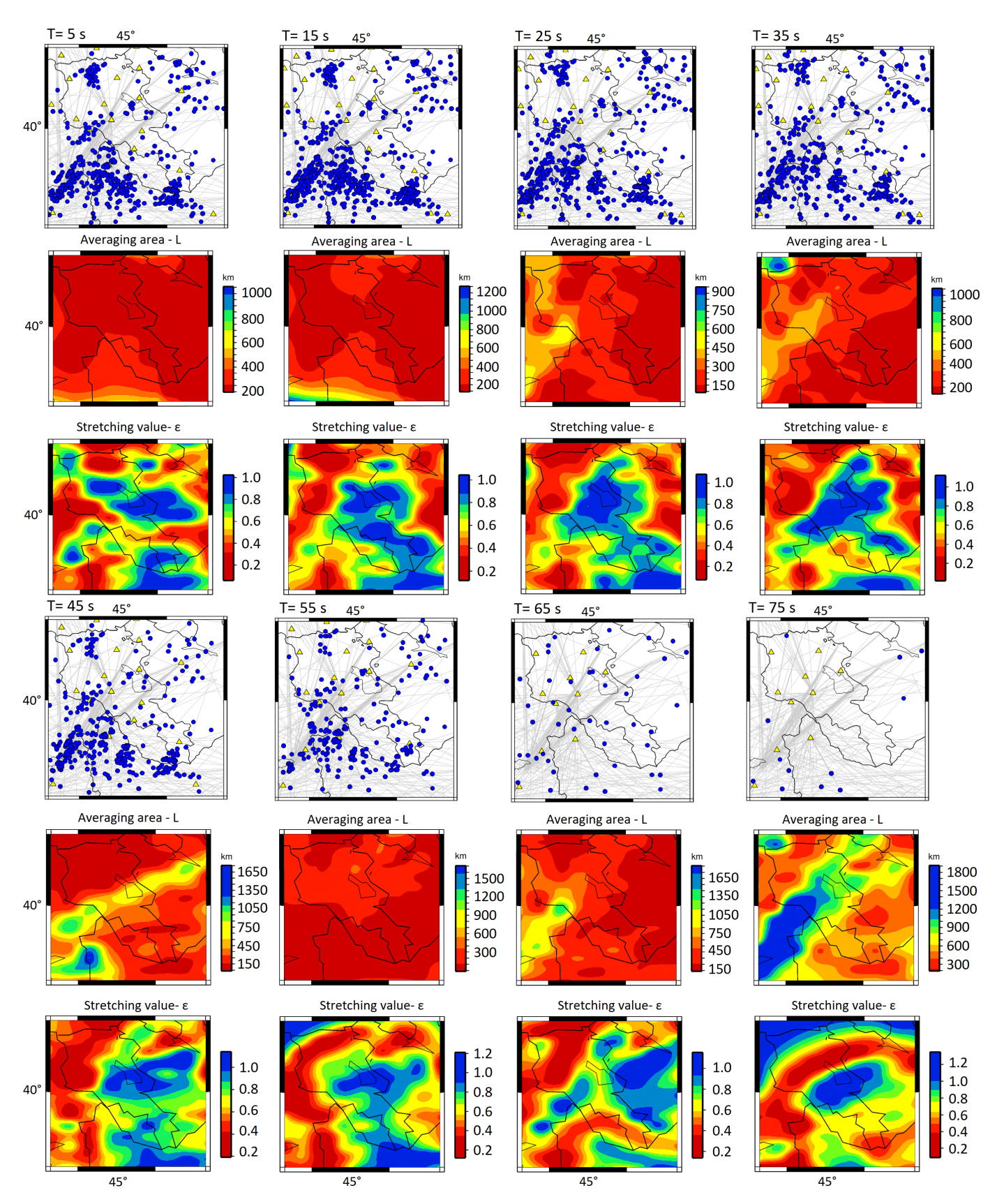


**Figure 3.** Some parameters influence the clarity of tomographic images, including the distribution of earthquakes (blue circles), seismic stations (yellow triangles), ray paths (gray crosshatch lines), stretching –  $\varepsilon$  (green-blue shades), and averaging area – L (red shades) maps for odd periods of 5–75 s in this study.

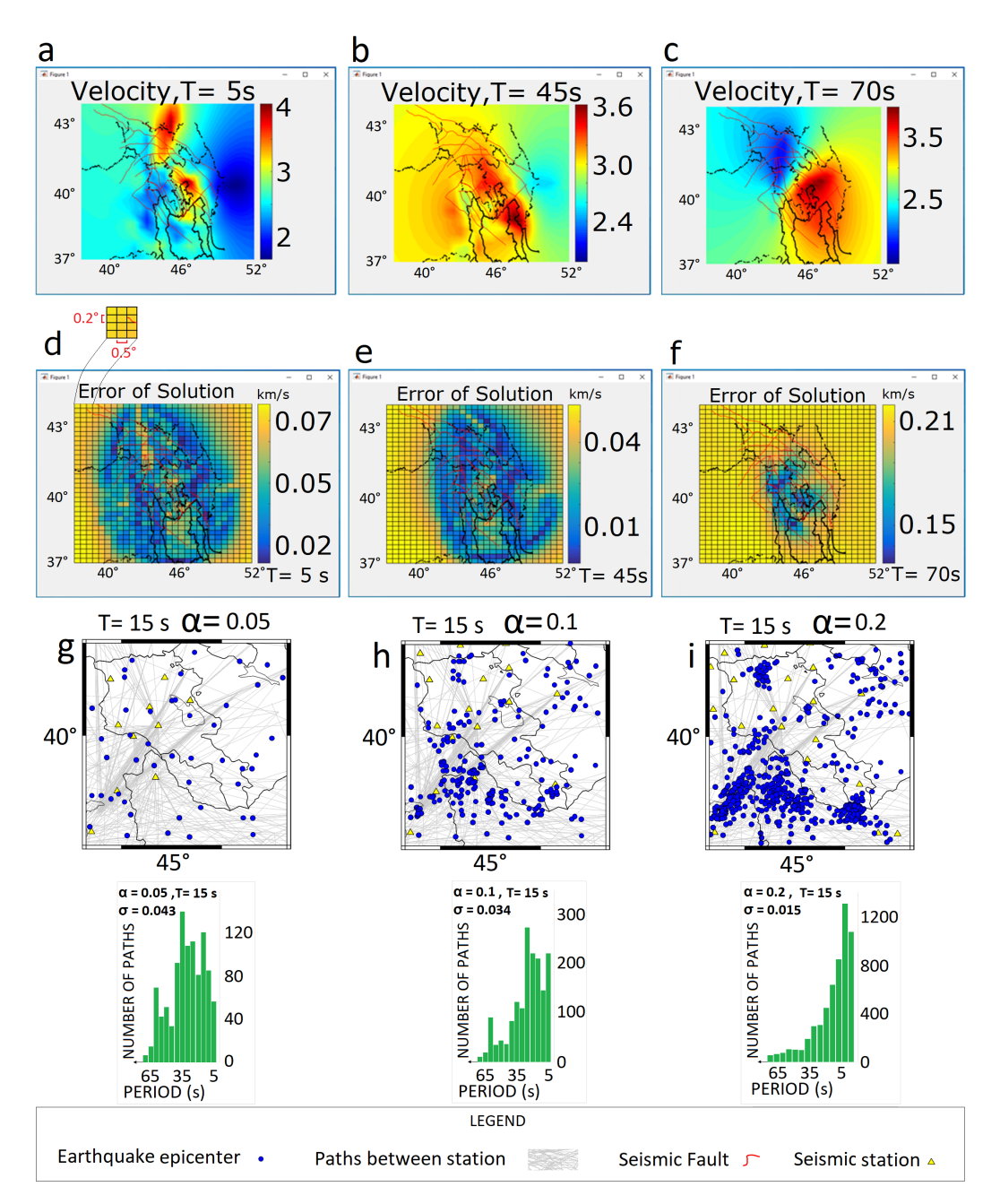


**Figure 3.** (continued) Figures d, e, and f show the error of solution and corresponding velocity maps (a, b, and c) with a cell spacing of  $0.2^{\circ} \times 0.5^{\circ}$  ( $20 \times 50 \text{ km}^2$  – top left corner of Figure d) for periods of 5, 45, and 70 s (generated by MATLAB software). The important role of regularization parameter ( $\alpha$ ) in smoothing and resolution of tomographic maps. Calculations of group velocity maps for several regularization parameter ( $\alpha$ ) are depicted (g, h, and i). Decreasing  $\alpha$  expresses a sharper solution region (an increase in solution error), while increasing  $\alpha$  leads to a smoother solution region by reducing the solution error. The parameter  $\sigma$  is an estimate of the standard error of the data. The histograms show the correlation changes between  $\alpha$ ,  $\sigma$ , and the number of rays in each period.

resolution of solutions defined by an oval centered at the point S(x = a, y = b). The values of a and b are the length of the small and large diameters of the ellipse, respectively. The resolution (averaging area – L) in each cell  $(20 \times 50 \text{ km}^2)$  of the study area is determined as L = (a+b)/2. The other parameter called stretching  $(\varepsilon)$  which is defined as  $\varepsilon = 2(a-b)/(a+b)$  and evaluates the dissimilarity of the coverage of ray space.

Figure 3 depicts the resolution parameters (L and  $\varepsilon$ ) for odd periods 5–75 s. Generally, large values of stretching ( $\varepsilon$  > 1) imply that the paths have a preferred trend, and  $\varepsilon$  is likely to be very small along this preferred direction. On the contrary, the small values

of  $\varepsilon$  imply that the paths are distributed (almost uniformly) along all directions; hence the resolution at any point can be demonstrated by the mean size of the averaging area (L). In this research, the value of  $\varepsilon$  was calculated equal to 0.66 (close to the light green shades) which indicates that for each direction the azimuthal distribution of the paths is sufficiently uniform and the resolution is almost the same.

In order to achieve optimal results, the data and seismic stations were increased across the Caucasus region, and a high-resolution 2D tomographic velocity model was calculated by inverting the paths of Rayleigh wave dispersion curves at 1050 nodes  $(35 \times 30 = 1050)$  using a grid with cell sizes of  $0.2^{\circ} \times 0.5^{\circ}$  or  $20 \times 50$  km<sup>2</sup> (Figure 3 continued d–f).

Chen et al. [2010] determined the statistical error margin of the solution due to source mislocation to be less than 0.03 km/s for the Rayleigh wave velocity. The solution error value is relatively higher for the areas marked with yellow color (Figure 3 continued d-f).

Inaccurate locating (mislocation) of the earthquake source (e.g., basic parameters of earthquakes – long., lat., mag., depth, ...) leads to errors in the dimensions of heterogeneities determined from resolution length or averaging area (L) maps. The (L), in the majority of geological units within the study area is approximately  $100-200\,\mathrm{km}$  (Figure 3), with the exception of marginal areas that exhibit low radiation coverage. The solution error varies between 0.015 and  $0.21\,\mathrm{km/s}$ ; however, in most regions of the study area (Armenia), these values are below  $0.3\,\mathrm{km/s}$  (Figure 3 continued, d–f).

#### 4. Methodology

## 4.1. Estimation of dispersion curves (group velocity)

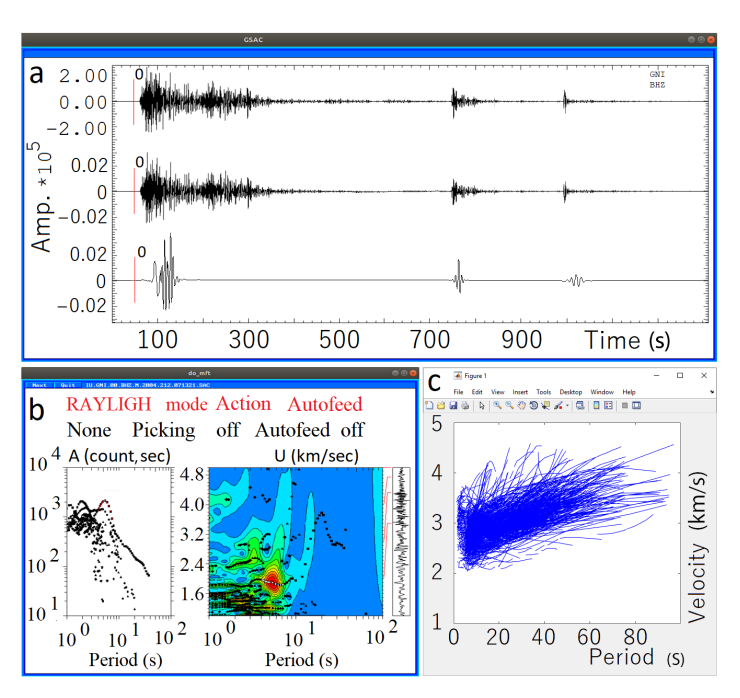


Figure 4. Different steps for determining the dispersion curve from fundamental mode of the Rayleigh wave (the red shade that has the lowest frequency and maximum energy) through the do\_mft package; a. Raw waveform, rotated horizontal component, and cleaned seismogram traces recorded in GNI (Garni) station in Armenia (from top to bottom, respectively). The vertical red lines with the number zero "0" above them indicate the onset of the wave arrival time – auto picked (pick-file) by SAC software; b. High-energy area (red shade) of the seismic signal for determining the dispersion curve using the do\_mft package and its spectral curves (left); c. The estimated dispersion curves for the period range of 5–80 s.

In the real Earth structure, Rayleigh waves can be observed on the vertical (Z) and radial components, while Love waves are detected on the transverse component. In the data processing procedure, the group velocity is determined by rotating the two horizontal components (EW and NS) of each Rayleigh wave time series along the great circle path to obtain the radial and transverse components (Figure 4a).

To measure the Rayleigh wave dispersion curves, a multiple filter method is employed. This involves filtering the original seismogram using a series of narrowband Gaussian filters [e.g., Bune, 1955; Dziewonski et al., 1969] with varying periods, applied to the broadband vertical component seismogram across multiple different periods [e.g., Herrmann, 1973]. In this way, the maximum amplitude at each period is picked on the envelope function, and the arrival time associated with this maximum amplitude is utilized to calculate the group velocity. This method generates a 2-D diagram representing signal power as a function of time or group velocity.

The initial step in determining surface wave dispersion curves involves conducting an exploratory analysis of the waveform data to identify events with acceptable signal-to-noise ratios (SNR > 3). Then, after rotating the components, several standard procedures (e.g., instrument response correction, removal of the mean and trend, temporal normalization, and spectral whitening of the band-pass filter) were applied to all waveform data (5–50 s). Subsequently, the dispersion curve for each path is obtained from the do\_mft diagrams. An example of this process is illustrated in Figure 4, which shows the determination of the dispersion curve for the vertical (Z)

component of the Garni (GNI) seismic station in Armenia. In this context, over 30,000 dispersion curves were processed using the do\_mft package (Figure 4c). Similarly, to measure Love wave dispersion curves, the same procedure can be applied to data that has been rotated in the transverse direction.

#### 4.1.1. Quality control of data and curves

As the number of seismic stations increases, the number of inter-station paths also rises. However, to obtain high-quality dispersion curves (group velocity), it is essential to apply data quality control criteria to identify and eliminate erroneous measurements. Consequently, not all paths can be utilized. For this purpose, the fundamental mode of the Rayleigh wave-which has the lowest frequency and the highest energy-is manually extracted using the do\_mft package.

This research employs several data selection criteria. First, events with  $M \ge 4$  were selected, while those with  $M \le 3.9$  were excluded due to the few number of dispersion points. Second, a Signal-to-Noise Ratio (SNR) >3 was utilized to analyze and establish a robust database in the time domain, which has minimal impact on the period ranges of 5–80 s in this study. Usually, in studies involving time series analysis (such as Multichannel Fourier Transform (MFT) and Time-Varying Technique (TVF) methods), a Signal-to-Noise Ratio (SNR) range of 10 to 100 s is eligible, while the data with low S/N is generally discarded due to low dispersion [Herrmann, 2013].

The third measure of solution quality is the residual travel time ( $\sigma$ ), which is assumed as an estimate of the standard error of the uncalculated random residuals. The  $\sigma$  parameter is the acceptable error range, that causes the dispersion curves with high error (outlier) to be removed. To mitigate the effect of large errors, residual data larger than  $3\sigma$  are rejected, and the tomography reconstruction process is then repeated [*Yanovskaya et al.*, 1998]. By selecting a regularization parameter of  $\alpha = 0.2$  for smoothing the maps, the standard deviation ( $\sigma$ ) remains relatively low. This indicates the stability of the method and reflects the probability density function of the observed data across different periods (Figure 3 continued – histograms).

#### 4.2. Two-dimensional tomography

As previously noted, this study employed a 2D linear inversion method on the data to create group velocity tomography maps. This approach is a generalized version of the classical 1-D method developed by [Backus and Gilbert, 1968] and further developed by [Ditmar and Yanovskaya, 1987], as well as [Yanovskaya and Ditmar, 1990]. In this method, time series data or travel time were calculated along various paths for each period using the do\_mft package. The distribution of group velocity  $V_x$  for each period can be approximated by minimizing the function presented in Equation 1:

$$\alpha \iint \left| \nabla_m(X) \right|^2 dX + \left( d - Gm \right)^T \left( d - GM \right) = \min. \tag{1}$$

Here,  $d_i = T_i - T_{i0}$  represents an input data vector, where t and  $t_0$  denote the observed and computed travel times along each path, respectively. G refers to the data kernel, and m(x) is defined as Equation 2:

$$\delta m(X) = (V^{-1}(X) - V_0^{-1})V_0 \tag{2}$$

By transforming the coordinate system, the solution for V(X) is found in the Cartesian coordinate planes defined by x = (x, y). Subsequently, this solution is transformed back into spherical coordinates.

The  $\alpha$  parameter controls the trade-off between smoothness and data fitting in the obtained phase velocity maps [*Yanovskaya et al.*, 1998]. Phase velocity maps are determined through a trial-and-error approach by testing several regularization parameters ( $\alpha = 0.05, 0.1, 0.2, \text{ and } 0.3$ ). An acceptable value of  $\alpha = 0.2$  was chosen, resulting in rel-

atively smoother maps with minimal solution error values. In this study, specialized MATLAB codes were employed to achieve minor solution errors by testing various  $\alpha$  values while simultaneously observing the beams passing through each cell with dimensions (cell spacing) of  $20 \times 50 \,\mathrm{km}^2$  (Figure 3 continued-g, h, i, and histograms).

Figure 3 continued (g, h, i, and histograms) illustrates the significant impact of the regularization parameter ( $\alpha$ ) in Equation 1 on the resolution of the 2D tomography images, including factors such as the number of paths per period, the distribution of stations and earthquakes, and the ray coverage between seismic epicenters and stations. This technique is also effective for addressing the non-uniform distribution of surface wave paths. Then, 2D tomography maps for Rayleigh and Love waves were plotted using GSAC and GMT software, along with specialized MATLAB codes on the Ubuntu operating system. These maps included parameters such as velocity, stretching ( $\varepsilon$ ), data density, averaging area (L), and dispersion curves across a period range of 5 to 80 s (Figures 3, 4, 5, and 7).

### 5. 5. Results and discussion (interpretation of obtained 2D tomography maps)

Employing the tomography method outlined in subsection 4.2, Rayleigh and Love wave group velocity maps for periods ranging from 5 to 80 s have been generated (Figures 5 and 7). These maps indicate that various periods are sensitive to seismic shear wave velocities at different depths, and longer-period waves demonstrating sensitivity to deeper layers or depths [*Urban et al.*, 1993].

Additionally, Figure 1a–b illustrates the active tectonic features and geological units of the study area, which are addressed in the interpretation of the presented 2D tomography maps. The minimum and maximum wave penetration depths are determined by Equation 3 and Figure 6d (sensitivity kernels).

Depth = 
$$\frac{2}{3}\lambda$$
, (3)

where  $\lambda = V/F$  is the wavelength, and V, F and T are velocity, frequency (F = 1/T), and period, respectively. It is important to highlight that the sensitivity kernels presented in Figure 6d are employed to interpret the tomographic maps at various depths and periods.

In this study, based on seismic tomography interpretation within the Earth [e.g., *Bedle and Lee*, 2009], the areas shaded in dark red and orange indicate low-velocity (slow) zones, while the dark blue, green, and yellow shades represent high-velocity (fast) zones (Figure 5). Therefore, the commentary of these tomography maps, considering the aforementioned characteristics and comparing them with results from previous tomography studies in the region regarding velocity anomalies at various periods and depths, is presented below. The tomography maps in this study are described for four categories: short, medium, long periods, and Love waves.

The sensitivity kernels (Figure 6d and Equation 3) indicate that shallow structures predominantly control dispersion at short periods, while deeper structures have a more significant impact on longer periods.

The short-periods (T = 5–25 s; Figure 6) indicate that Rayleigh wave tomography velocity maps sample the entire upper and lower crust (according to the sensitivity kernels Figure 7b Depth  $\approx$  7 to 58 km and Equation 3) and comprise information about shallow geologic structures related with upper crust (e.g., sedimentary basins, uplifts, and volcanic complexes) and lower crust (e.g., Moho). The short periods (T = 5 - 25 s; Figure 5) reveal that the Rayleigh wave tomography velocity maps sample both the entire upper and lower crust (as indicated by the sensitivity kernels in Figure 6d, with depths ranging from  $\sim$  7 to 58 km). These maps provide insights into shallow geological structures associated with the upper crust (e.g., sedimentary basins, uplifts, and volcanic complexes) as well as features of the lower crust (e.g., the Moho).

The patterns of the tomography maps at 5, 15, and 25 s (Figure 5) are similar, with the exception of the western slope of the Aragats stratovolcano area, where a low-velocity anomaly is observed.

Tomographic maps illustrated in Figures 5, A1, and A2 for periods of T=5 s and 10 s reveal a notable high-velocity anomaly along the South Azerbaijan, Sheki, Tbilisi, Grozny (Terek basin), TAL (Talesh), BM, and Elbrus-Aragats-Kazbek volcanoes, which are surrounded by low-velocity anomalies in regions such as SCB, KD, RB, Alazani, EBSB, EAAC, and the eastern part of NTF.

Alternatively, the observed lower velocities in the upper crust of the EAAC and northwest Iran, areas that lack a significant sedimentary basin, can be attributed to extensive zones of partial melting in the crust. This phenomenon is likely a result of the interaction between the hot asthenosphere and a shallow magma source within the EAAC [e.g., *Aydın et al.*, 2005; *Keskin*, 2003].

Certainly, the presence of thick sediments is responsible for the low group velocities observed in basins (e.g., SCB, which has a depth of  $\sim$  7 to 15 km; [*Jackson et al.*, 2002]). Additionally, the low-velocity zone beneath volcanic complexes, such as Aragats, may be attributed to the high temperatures of the volcanic rocks or the existence of shallow magma chambers.

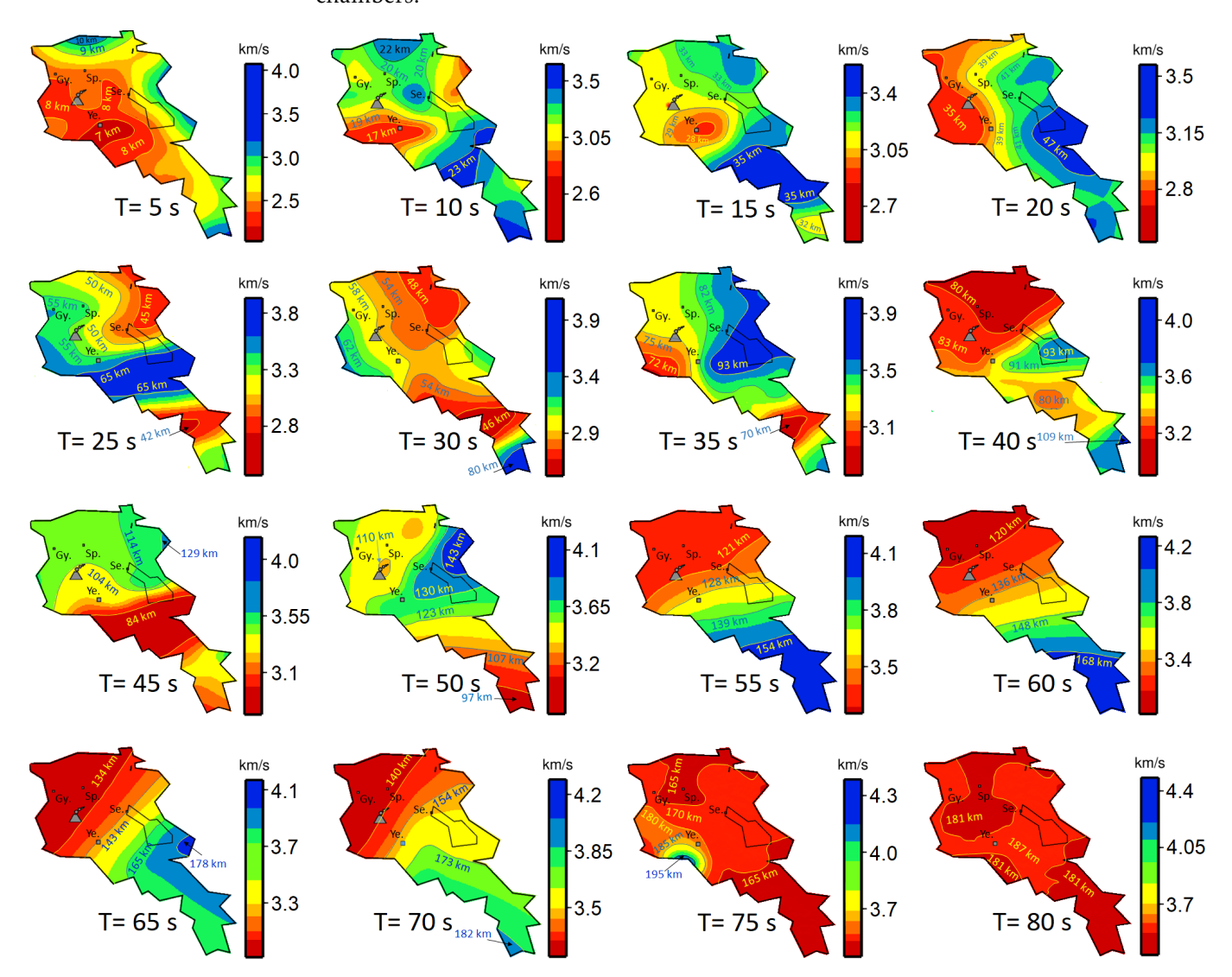


**Figure 5.** Rayleigh wave group velocity tomography maps for periods of 5–80 s. Abbreviations: Gy. – Gyumri, Sp. – Spitak, Se. – Sevan, and Ye. – Yerevan.

The Gegham Volcanic Group in the CAB also aligns with a low-velocity anomaly; however, the Aragats stratovolcano is an exception, as it falls under a high-velocity anomaly. This is likely due to its long dormancy, indicating no volcanic activity for over half a million

years [e.g., *Koulakov et al.*, 2012]. In contrast to the results of previous studies such as [*Koulakov et al.*, 2012], the tomography map at T=15 s of this study reveals a small low-velocity zone on the northwest slope of the Aragats volcano at a depth of  $\sim 27$  km, which is different from the results of other studies. We infer that this observation may be attributed to the dynamics of molten material located beneath the volcano.

The small orange shades observed at short periods in this study, located beneath volcanoes such as Elbrus, Tendurek, and Ararat at depths of approximately 27–37 km, align with findings from [*Milyukov et al.*, 2018]. Their research indicated the presence of a magma chamber at depths of 1–8 km, along with an extended magma source situated between 15–40 km beneath the eastern summit of Elbrus.

In the altitudes of LC, TAL, Elbrus, GC, and Kars, high- and low-velocity anomalies are observed across short (T < 25 s), medium (T > 45 s), and long (T > 50 s) periods. These anomalies can be interpreted as a relative thickening of the crust.

Some studies, including [Bochud, 2011], have recognized numerous abundant oil and gas fields (hydrocarbon resources) within the Paleogene and Neogene strata of the central Armenia Troughs, which encompass the Sevan, Sevan trough, Vokchaberd, Avan, Yerevan, and Yeghvard regions. The 2D tomography maps produced in this research for periods of 5 s and 10 s demonstrate a broad low-velocity zone in the Central Armenia Block (CAB). Consequently, we suggest that these low-velocity maps (dark red shades) provide compelling evidence for the interactions involving these chemical resources.

The Avon Salt-Dome region, located between Harazdan and the Vokchaberd Plateau, has exhibited potential for oil in the Middle Miocene section [e.g., *Klett*, 2016]. Therefore, the low-velocity anomaly identified in the Central Armenia Block (CAB) in this study outlines these oil and gas regions, including Yerevan, Sevan, Gavar, and Martuni. This suggests that these areas should be considered for meeting the country's future energy requirements.

In this study regarding the Moho discontinuity, the presence of low-velocity anomalies observed within the 15 to 20-s period range ( $\sim$  22 < Depth < $\sim$  42.66 km) may be a strong reason. In this context, research by [Sun et al., 2012] identified Moho depths ranging from 20 to 40 km across various geological units in the Caucasus, which closely aligns with the findings of this study (Figure 6a and d).

The existence of low-velocity zones in certain sections of the Tabriz-Balykgel, Garni, PSS, and Akerin faults (Figures A1 and A2) may be attributed to thermal activities resulting from the fracturing of fault rocks or basaltic eruptions during the Quaternary period [Lebedev et al., 2013].

In this study, the velocities of Rayleigh waves at short periods (5–15 s), which provide the information relative to the upper-crust (Figure 6d), are essentially sensitive to shallow geological features such as sedimentary basins (troughs), topography (uplift), and potentially volcanic structures. The velocities of Rayleigh waves at periods of 20–25 s provide insights into the lower crust, including the Moho discontinuity. Similarly, the Love waves (Figure 7) exhibit characteristics that are somewhat comparable to those of the short-period Rayleigh waves.

For medium periods (T = 30-50 s; see Figure 5), and based on the curves in Figure 7d, Rayleigh waves provide insights into the velocity structure of the lower crust and uppermost mantle. Consequently, in continental regions, low velocities at these periods indicate either a thick crust overlying a normal continental lid or thin and weak lithospheric mantle beneath a normal crust. While, high velocities typically indicate the presence of a normal continental crust situated over a stable, thick layer or an oceanic-like lid. Indeed, at periods  $\geq 30$  s or more, the wave velocity models enable us to delineate various lithospheric structures and the crustal depth in the region.

As a result, Rayleigh waves exhibit increased sensitivity to crustal thickness, which encompasses both LC and GC mountain ranges in this study. In these areas with thick crust, the group velocities are more sensitive the slow crustal velocities compared to the fast velocities of the mantle. This feature is quite obvious in the Talesh region of NW Iran,

as well as in the NAB-CAB-SAB (LC), and GC (from west to east). For instance, at 50 s, there is a noticeable arc of low-velocity along the NAB-CAB-SAB or LC (North Armenia Arc) and EAAC (Ararat-BM), which extends into the NW Iran (Urmian Arc) mountains. At 30–45 s, the eastern GC, PT, RB (Georgia), and EBSB continue westward, as illustrated in Figures 5, A1, and A2.

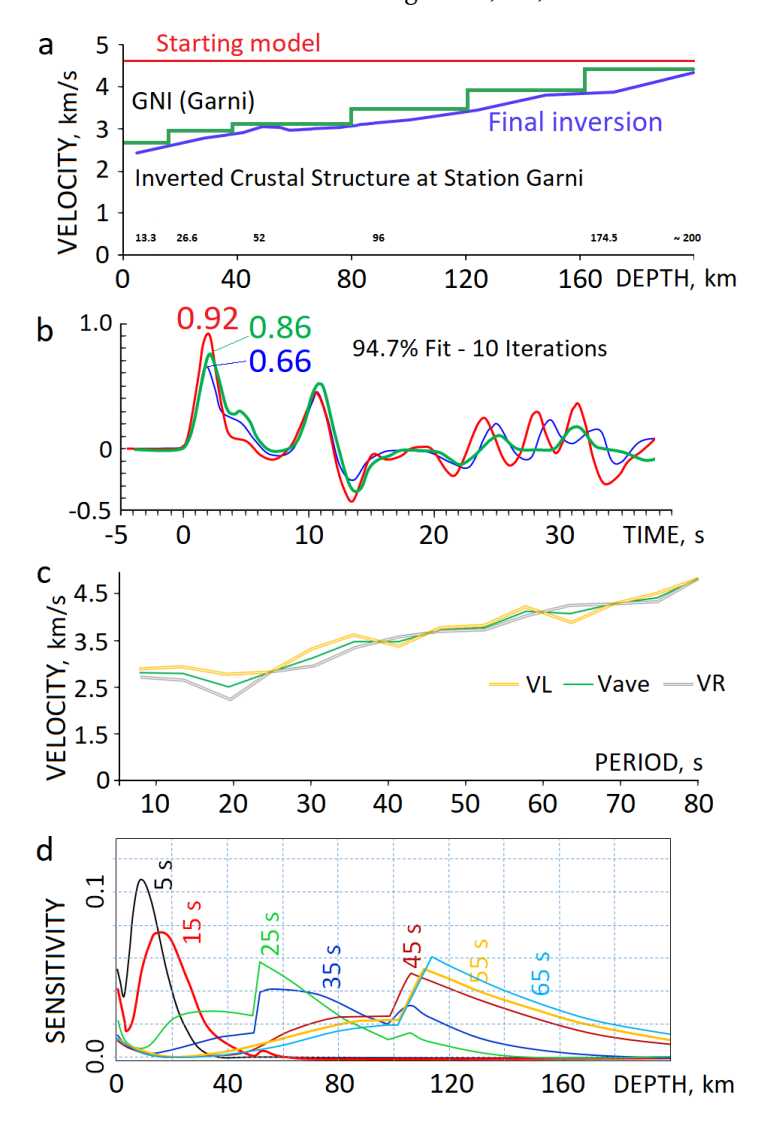


Figure 6. a. The velocity model beneath station GNI (Garni) was determined by inverting the stacked receiver function generated in (b) after 10 iterations. The structure has been perturbed from the initial model (solid red line) to the model indicated by the solid blue line; b. For each model, the original receiver function (red line) and the receiver function for the joint inversion model (blue) are shown. Additionally, the synthetic receiver function produced by the model (green). It is evident that there is a strong correlation between the two sets of curves. In nearly all time intervals, the peaks and valleys of both curves align closely (parallel) with one another; c. Variation curves of Rayleigh (VR) and Love (VL) wave velocities along with their average (Vave) velocity; d. Computed velocity sensitivity kernels for the fundamental mode of Rayleigh waves over periods ranging 5–65 s.

In contrast, due to the physical processes occurring within the Earth that contribute to magma generation, the velocity values increase towards the SAB, NW Iran, and EAAC. This is attributed to the fast mantle velocities and the presence of partial melting zones inside the crust, as well as a very shallow lithosphere-asthenosphere boundary (LAB) of ~ 70 km [e.g., *Skobeltsyn et al.*, 2014], which is supported by a hot asthenosphere associated with volcanism originating from the uppermost mantle. It is important to highlight that the high-velocity observed in the lower crust of the SCB compared to NW Iran is likely due to the oceanic source of the lower crust. Overall, in these areas with thick crust, the group velocities are more sensitive to the slow crustal velocities rather than the fast mantle velocities.

We attribute that the propagation of the high-velocity anomaly in the lower crust within the transition zone from the SCB and KB to NW Iran and the SAB reveals that the high-velocity (3.6 km/s) observed beneath Talesh, the Transcaucasian Massif (TCM), and Kazbek in the eastern GC is likely a result of the ongoing subduction (underthrusting) of the Kura Basin lithosphere beneath the Scythian platform, due to the presence of a stable and thick mantle in the eastern Caucasus. On the contrary, the low-velocity dispersion (2.4 km/s) observed beneath the SAB-LC, EAAC, Tabriz Fault, Sahand volcano, and BM may result from a very thin lithosphere (< 100 km) or a thin mantle.

By comparing the lower crust velocities in the SCB and KB (at  $T=40 \, \mathrm{s}$  and 50 s) with those in NW Iran (at  $T=50 \, \mathrm{s}$ ), we observe different origins for the lower crust in the basin, likely indicating an oceanic source, due to the significantly higher velocities relative to NW Iran. In this context, Mortezanejad [Mortezanejad et al., 2018] proposed evidence of the lower crust of the SCB being under-thrust beneath NW Iran, while the middle crust remains locked.

According to the findings of Avagyan [Avagyan et al., 2010], upper Devonian and Permian petroleum source rocks (marine clastic and carbonate rocks) are exposed in Nakhchivan and are believed to also exist in Armenia. Consequently, we associate the low-velocity tomography maps of the Nakhchivan and Syunik-Gegham-Vardenis (SAB) highlands with the results of Avagyan [Avagyan et al., 2010].

In general, this study state that the observed low-velocity in the western GC and high-velocity in the east-ern GC (at medium periods) may be indicative of a weak,

hot, and thermally altered lithosphere beneath the western GC, in contrast to a more elastic and cooler lithosphere in the eastern GC [e.g., *Ruppel and McNutt*, 1990].

The upper mantle low-velocity zone (LVZ) is a depth where there is a slight pause or break (interval) in seismic velocity as one transitions from the lithosphere to the asthenosphere, attributed to the very small percentage of melt present in the asthenosphere [e.g., *Sugden et al.*, 2018]. The LVZ is found at a relatively consistent depth of 100 km (specifically 104 km in this study, as shown in Figure 6; [*Abrehdari et al.*, 2022, 2023]) beneath the continental regions of the world [*Thybo*, 2006]. According to [*Abrehdari et al.*, 2022, 2023], the wide and prominent low-velocity zone in the SAB, Garni, and Zangezur faults (Figures A1 and A2) reveals interactions between the LAB or LVZ discontinuities, resulting from a rapid change in velocity from very high ( $v = 4.75 \, \text{km/s}$ ) to very low ( $v = 3.2 \, \text{km/s}$ ) at  $t = 5.5 \, \text{s}$  and 60 s.

For long periods (50–80 s; depth  $\sim$  200 km; Figures 5 and 6d), Rayleigh waves likely begin to predominantly sample the upper mantle (mantle lid). The inversion results (tomographic maps) for periods ranging from 55–80 s almost display a consistent and uniform pattern (strong similarities). Although, at the longest periods of study (65–80 s), there is inadequate path coverage to generate reliable maps. In this case, velocity anomalies in the oceanic regions remain high, with the exception of slow-velocities observed along the oceanic ridges [e.g., *Pasyanos et al.*, 2001].

Tomography maps within these periods indicate that the NAB, CAB, and SAB blocks (the entire Armenia-LC region), throughout the western Great Caucasus (GC) except for the eastern GC, NW Iran, TAL, and SCB, are dominated by ultra-low group velocity (dark red shades), which this phenomenon may be attributed to the thin lithospheric lid of the mantle (Figures 5, A1, and A2).

Summarily, these maps (at a depth of  $\sim$  180–200 km) provide a rundown of the upper mantle structures and recognized tectonic features. It can be conclusively stated that the mantle lithosphere is either very thin or nearly absent beneath the Caucasus and its surrounding areas. Because of this process, the overheated asthenosphere appears to be very close to the bottom of the crust, facilitating magma transport and contributing to the formation of active volcanic fields in the Caucasus [e.g., *Zabelina et al.*, 2016].

For these deep regions, the active subduction (such as detached slabs), tectonic interactions from east to west of the Caucasus, and the occurrence of deep earthquakes (e.g., 2015-09-12\_02:08:49, depth = 121.66 km, eastern Caucasus) present a large seismic hazard (with potential magnitudes  $\sim$  8). These factors, along with lithospheric interactions, also play a role in the feeding mechanisms of volcanoes.

Additionally, the deep low-velocity zones (indicated by dark red shades in the SAB, CAB, and SAB) have raised concerns among seismologists regarding certain physical properties of these areas. These include the lithospheric-asthenospheric boundary (LAB), low-velocity zones (LVZ), rigidity, wax-like effects, variations in wave velocity, magma chambers beneath the plateau, and a notable degree of partial melting. Together, these factors suggest the potential for future volcanic activity [Abrehdari et al., 2022].

Furthermore, ultra-low velocity anomalies may be linked with active plate tectonic processes, a very thin lithosphere, and the formation and intrusion of hot asthenospheric diapirs (~ 1400°C at a depth of 150 km). Conversely, ultra-high velocity zones can be associated to the rejuvenation of the upper mantle due to upwelling mantle metasomatic fertilization of the upper cratonic mantle [e.g., *Beccaluva et al.*, 2007; *Thybo*, 2006].

Figures 5 and 7 illustrate the 2D Rayleigh and Love wave group velocity tomography maps of Armenia for periods ranging from 5 to 80 s with different topographic coefficients. These maps compare the distinct distribution of velocity anomalies across different geological units in Armenia during short, medium, and long periods. The velocity tomography images for Love waves (Figure 7) demonstrate a pattern that closely resembles that of the Rayleigh wave images (Figure 5).

Although the quality and resolution of Rayleigh wave velocity maps are superior to those of Love waves due to the larger number of paths and data, it is important to note that the energy distribution of Love and Rayleigh waves differs, and they may not be generated together in all locations.

As shown in Figures 5 and 7, fluctuations in velocity ranging from 2.3 to 4.5 km/s are clearly visible in the Rayleigh and Love wave tomography maps for short and medium periods, extending from the upper crust to the lower crust. While there is no substantial difference in the dispersion of Love and Rayleigh waves at long periods and long wavelengths, both reveal a slow and uniform velocity distribution ranging from 3.53 to 4.77 km/s in the upper mantle or mantle lid regions.

The Love wave tomography maps (Figure 7), which are more sensitive to shallow structures, exhibit features that are somewhat similar to those of the short-period Rayleigh waves (Figure 5). Also, according to Rahimi [*Rahimi*, 2010], in Love wave dispersion the energy is concentrated in the tangential horizontal plane.

As noted,  $\sim 27,000$  components for Rayleigh waves and  $\sim 22,000$  for Love waves were obtained from the seismic stations. Therefore, the resolution of the Love wave images is poorer to that of the Rayleigh waves, likely due to the smaller number of measurements and the lower signal-to-noise ratio (SNR) in the data.

In contrast to Rayleigh waves, Love waves appear fairly similar across a wide range of frequencies (periods). This may be attributed to the sensitivity of Love waves to shallow surface structures, at short and even longer periods.

In addition, for deep water regions, the lateral variations in Rayleigh wave velocities exceed those of Love waves due to the influence of the water layer, which this leads to multipathing and allows different spectral components to propagate along different paths [e.g., *Yanovskaya et al.*, 1998].

Short-period Love waves (T = 5-25 s) highlight shallow sedimentary basins (depressions). In the medium periods ranging T = 30-50 s, the velocity structures in the deeper sedimentary basins are still prominent, and slow-velocity anomalies are primarily confined to the deepest basins, such as the SCB. Sensitivity to crustal-thickness, including heights and mountain ranges, begins at the longest periods (T = 55-70 s), where slow-velocities linked to the Greater Caucasus (GC) and Lesser Caucasus (LC) are observable. As a finding, this research concludes that slow Love wave group velocities are typically dominate in deep basins across all short, medium, and long periods. This indicates that Love wave is more tend to penetrate and extend into shallower regions than the Rayleigh wave.

## 6. Conclusions

A seismic model of the sub-Caucasian crust was developed based on the inversion of 2D tomographic maps of Rayleigh and Love waves from earthquakes in the region, as recorded by regional seismic networks in the Caucasian republics. The results of Rayleigh and Love wave group velocities in this study, covering periods from 5–80 s, provide a more accurate assessment of velocity changes compared to earlier studies in the region, thanks to the incorporation of new permanent stations.

This paper provides new perspectives on the tectonic and geodynamic processes influencing the Armenia region by utilizing a significant data set and advanced high-resolution 2D surface wave tomography technique, potentially leading to new insights into the Armenian area and its surroundings.

Upon reviewing the findings for the shortest periods (T = 5-25 s), it is evident that the velocity maps align closely with the surface geology and key topographic features. In this context, basin and depression areas are represented as low-velocity anomalies, while uplifted and mountainous regions appear as high-velocity zones. For Love and Rayleigh waves, high-velocity anomalies are observed in the North Armenia Block (NAB). At a 15-s period, a small low-velocity anomaly is detected on the NW slope of the Aragats volcano at a depth of  $\sim 27$  km, which differs from the findings of other studies. Additionally, during these periods, the high-velocity anomaly in the Greater and Lesser Caucasus likely indicates a rigid crustal block associated with uplift, whereas the low-velocity anomaly reflects the remnants of sedimentary basins. In this study, the identified low-velocity area (shown in

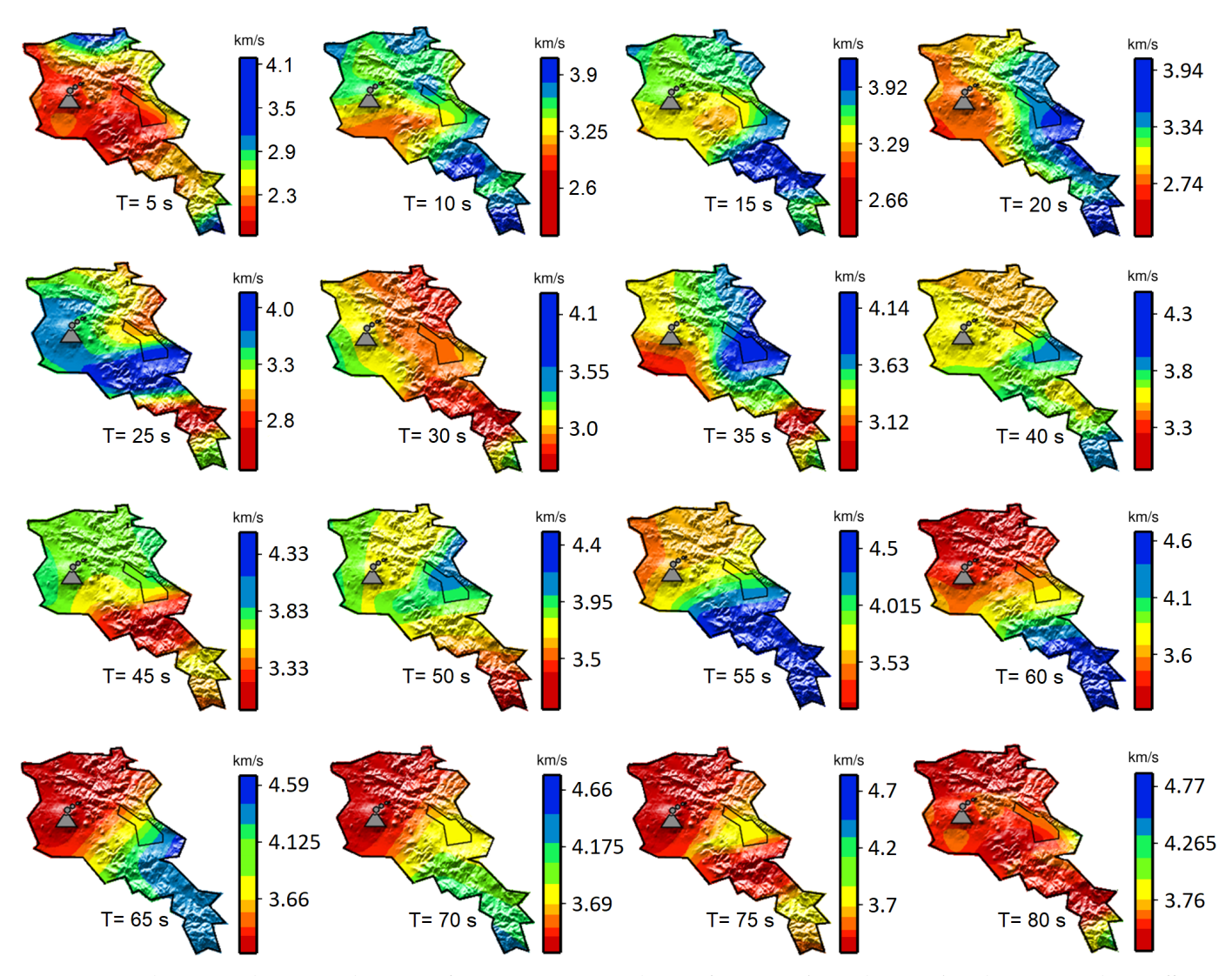


Figure 7. Two-dimensional tomography maps of Love wave group velocity of Armenia (periods 5–70 s) with a topographic coefficient 1.5 and  $\sim$  22,000 vertical (Z) components of the processed dispersion curves. The gray triangle illustrates the position of Aragats stratovolcano.

dark red) at periods of 5, 10, and 15 s in the Central Armenia Block (CAB) corresponds well with the findings of the previously mentioned studies on oil and gas fields.

At the intermediate periods (T=35-55 s) of this study, low-velocity anomalies are thought to be linked to and aligned with the underlying crustal layer (i.e., a very shallow LAB) and a hot asthenosphere. On the other hand, high-velocity regions typically suggest the presence of standard continental crust situated over a stable, thick, or oceanic-like lid. At these periods, strongly deformed areas of Great and Lesser Caucasus (especially most Cenozoic volcanic centers) are mostly associated with low-velocity patterns representing thickened part of the crust and strong fracturing of rocks [e.g., *Zabelina et al.*, 2016].

Long-period tomography maps for Love and Rayleigh waves in the NAB and CAB reveal ultra-low velocity anomalies, mainly attributed to a thin lithosphere or the absence of a lithospheric mantle. In contrast, ultra-high velocities may be associated with the concentration of liquids in the chamber, a lack of hot asthenospheric diapirs, or the presence of a hard and thick crust covered by heights.

The presence of volcanic groups such as Gegham, Elbrus, and Kazbek, situated between extensive high-velocity segments at various periods, suggests that the delamination of the mantle occurred as a result of continental collision in the Caucasus region. This led to the formation of an overheated asthenosphere near the bottom of the crust, which

facilitated the melting of crustal materials, ultimately giving rise to recent volcanic activity in both the Great and Lesser Caucasus regions [e.g., *Zabelina et al.*, 2016].

The 2D images (Figure 7) indicate that the Love Wave consistently tends to measure shallow depths (upper crust) across all short, medium, and long periods.

Acknowledgments. Special thanks to the Iranian Seismological Center (IRSC), the International Federation of Digital Seismograph Networks (FDSN), the Incorporated Research Institutions for Seismology (IRIS), and the Iranian National Seismological Network (INSN) for providing Earthquakes Data utilized in this study. The authors express their gratitude to Wessel and Smith, whose GMT software was instrumental in creating many of the figures presented in this paper. The authors would like to extend their gratitude to the Institute of Geophysics at the University of Tehran for supporting and managing this study in the framework of the educational mission (2016–2018). The authors would like to extend their sincere appreciation to Professor T. B. Yanovskaya for generously providing her tomographic software and for offering insightful guidance on surface wave tomography.

# Appendix A

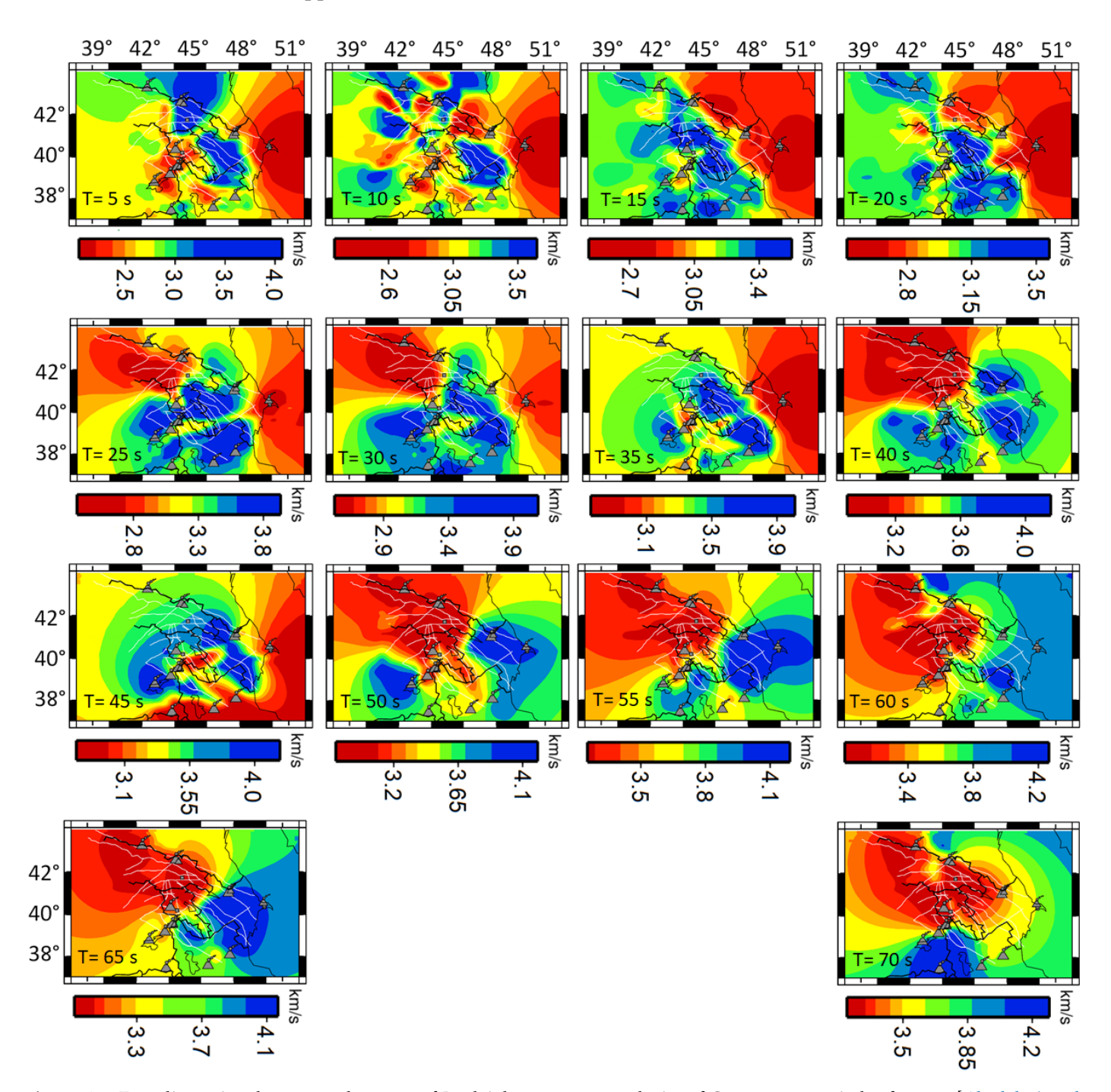


**Figure A1.** Two-dimensional tomography maps of Rayleigh wave group velocity of Caucasus at periods of 5–70 s [*Abrehdari et al.*, 2022, 2023].

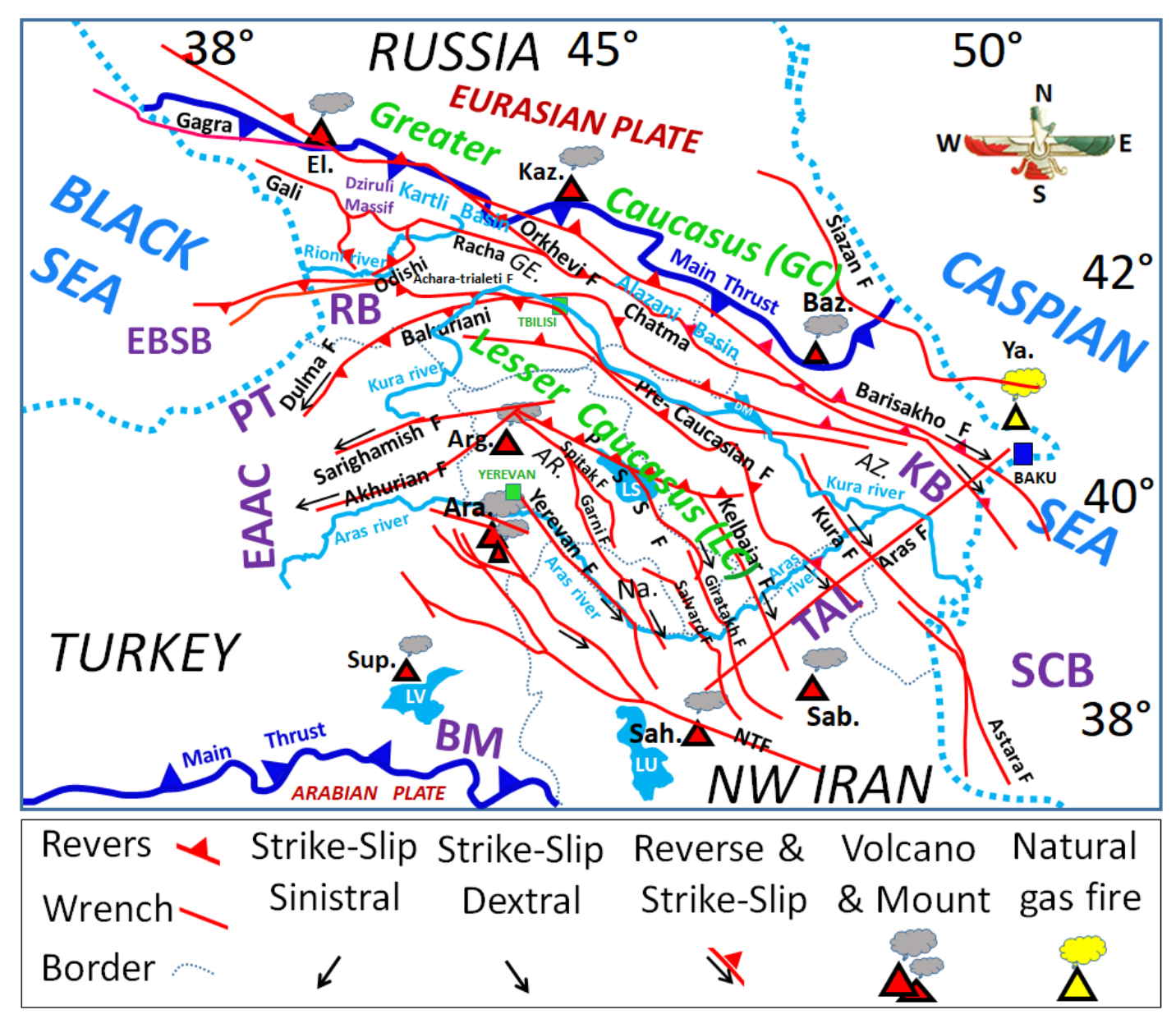


**Figure A2.** Major faults and active tectonic features of the collision zone of the Central Eurasian-Arabian and geological units discussed in the interpretation of 2D tomography maps of this study. Abbreviations: F – fault, Sab. – Sabalan, Sah. – Sahand, Sup. – Suphan, Ara. – Ararat, EAAC – East Anatolian Accretionary Complex, Arg. – Aragats, El. – Elbrus, Kaz. – Kazbek, Baz. – Bazarduzu, Ya. – Yanardag (natural gas fire on a hillside), RB – Rioni Basin, PT – Pontide, BM – Bitlis Massif, TAL – Talesh, KB – Kura Basin, LV – Lake Van, LU – Lake Urmia, LS – Lake Sevan, DM – Mingachevir Dam, SCB – South Caspian Basin, EBSB – Eastern Blake Sea Basin, Na. – Nakhchivan, Go. – Georgia, Az. – Azerbaijan, Ar. – Armenia, and PSSF – Pambak-Sevan-Syunik Fault. The thick black line denotes major plate boundaries in Caucasus. The seismic sources (faults) of the Caucasus are retrieved from Adamia [*Adamia et al.*, 2011].

Table A1. Information of events and stations for TEc measurements

Station Code	Station name	Longitude	Latitude	Network Code	Data Center Website
GNI/GSS	Garni, Armenia	44.7241	40.1341	IU (IRIS/USGS)	A0: National Seismic Network of Armenia https://www.fdsn.org/networks/ ?initial=G
AGVN	Aghvani	46.318143	39.359078	FDSN	IRISDMC https://www.fdsn.org/networks/ detail/A2/
ARZK	Arzakan	44.589914	40.428408	_	_
KCHK	Khachik	45.199504	39.610717	_	_
LRNG	Lernagog	43.873974	40.258703	_	_
SHMT	Shamut	44.804487	40.943472	_	_
SVZR	Sevadzayr	45.471962	39.920301	_	_
TTJR	Ttujur	45.365255	40.597151	_	_
ZRSH	Zarishat	43.67155	40.990359	_	_
GANJ	Ganja, Azerbaijan	46.3297	40.6519	IU (IRIS/USGS)	AB: National Seismic Network of Azerbaijan https://www.fdsn.org/networks/ detail/AB/
QZX	Qazah, Azerbaijan	45.3721	41.0481	IU (IRIS/USGS)	_
ZKT	Zakatala, Azerbaijan	46.6311	41.6411	IU (IRIS/USGS)	_
DIGO	KARS, TURKEY	40.4147	43.3742	IU (IRIS/USGS)	TU: National Seismic Network of Turkey (DDA) https://www.fdsn.org/networks/ detail/TU/
HAKT	HAKKARI, TURKEY	43.7071	37.5579	IU (IRIS/USGS)	_
KARS	KARS, TURKEY	43.0937	40.6152	KO (IRIS/USGS)	_
VANB	Gevas, Van sir	39.57798	28.63232	IU (IRIS/USGS)	TK: National Strong-Motion Network of Turkey (TR-NSMN) https://www.fdsn.org/networks/ detail/TK/
TASB	Tefenni, Burdur	37.3160	29.7791	IU (IRIS/USGS)	_
TAHR	_	47.0513	38.4894	IRSC	Iranian Seismological Center (IRSC) http://irsc.ut.ac.ir/istn.php
TBZ	Tabriz	46.1498	38.2348	IRSC	
TVRZ	_	46.6675	38.5042	IRSC	_
MAKU	Maku (Urmia)	44.6829	393550	INSN	http://www.iiees.ac.ir/en/iranian- national-broadband-seismic- network/

#### References

- Abrehdari, S. H., A. S. Hossein, J. K. Karapetyan, et al. (2022), The Caucasus Territory Hot-Cold Spots Determination and Description Using 2D Surface Waves Tomography, *Russian Journal of Earth Sciences*, 22(5), ES5004, https://doi.org/10.2205/2022ES000814.
- Abrehdari, S. H., A. S. Hossein, J. K. Karapetyan, et al. (2023), Tectonic Activities Description in the Ongoing Collision Zone of the Eurasia-Arabia Plates Using 2D Surface Waves Tomography, *Russian Journal of Earth Sciences*, 23(2), ES2004, https://doi.org/10.2205/2023ES000835.
- Adamia, S., G. Zakariadze, T. Chkhotua, et al. (2011), Geology of the Caucasus: A Review, *Turkish Journal of Earth Sciences*, 20(5), 489–544, https://doi.org/10.3906/yer-1005-11.
- Adamiya, S. A., M. A. Alekhidze, B. K. Balavadze, et al. (1992), The Caucasus: Integrated Geophysical Investigations of the Lithosphere, *International Geology Review*, 34(3), 249–263, https://doi.org/10.1080/00206819209465601.
- Avagyan, A., M. Sosson, A. Karakhanian, et al. (2010), Recent tectonic stress evolution in the Lesser Caucasus and adjacent regions, *Geological Society, London, Special Publications*, 340(1), 393–408, https://doi.org/10.1144/SP340.17.
- Aydın, I., H. I. Karat, and A. Koçak (2005), Curie-point depth map of Turkey, *Geophysical Journal International*, 162(2), 633–640, https://doi.org/10.1111/j.1365-246x.2005.02617.x.
- Backus, G., and F. Gilbert (1968), The Resolving Power of Gross Earth Data, *Geophysical Journal International*, 16(2), 169–205, https://doi.org/10.1111/j.1365-246x.1968.tb00216.x.
- Beccaluva, L., A. Azzouni-Sekkal, A. Benhallou, et al. (2007), Intracratonic asthenosphere upwelling and lithosphere rejuvenation beneath the Hoggar swell (Algeria): Evidence from HIMU metasomatised lherzolite mantle xenoliths, *Earth and Planetary Science Letters*, 260(3–4), 482–494, https://doi.org/10.1016/j.epsl.2007.05.047.
- Bedle, H., and S. V. D. Lee (2009), S velocity variations beneath North America, *Journal of Geophysical Research: Solid Earth*, 114(B7), https://doi.org/10.1029/2008jb005949.
- Bochud, M. (2011), Tectonics of the eastern greater caucasus in Azerbaijan, Université de Fribourg DOKPE.
- Bune, V. I. (1955), On the classification of earthquakes based on the energy of elastic waves emitted from their source, *Academy of Sciences of the Tajik SSR*, 14.
- Chen, Y., J. Badal, and J. Hu (2010), Love and Rayleigh Wave Tomography of the Qinghai-Tibet Plateau and Surrounding Areas, *Pure and Applied Geophysics*, 167(10), 1171–1203, https://doi.org/10.1007/s00024-009-0040-1.
- DeMets, C., R. G. Gordon, D. F. Argus, and S. Stein (1990), Current plate motions, *Geophysical Journal International*, 101(2), 425–478, https://doi.org/10.1111/j.1365-246x.1990.tb06579.x.
- Ditmar, P. G., and T. B. Yanovskaya (1987), Generalization of Backus-Gilbert method for estimation of lateral variations of surface wave velocities, *Izvestia*, *Phys. Solid Earth*, 23(6), 470–477.
- Dziewonski, A., S. Bloch, and M. Landisman (1969), A technique for the analysis of transient seismic signals, *Bulletin of the Seismological Society of America*, 59(1), 427–444, https://doi.org/10.1785/bssa0590010427.
- Echle, W. (1974), Zur Mineralogie und petrogeneses jungtertiarer tuffitischer Sedimente im Neogen-Becken nördlich Mihalıççık (Westanatolien, Türkei), *Neues Jahrbuch für Mineralogie Abhandlungen*, 121, 43–84 (in German).
- Eppelbaum, L., and B. Khesin (2012), Tectonical-Geophysical Setting of the Caucasus, in *Geophysical Studies in the Caucasus*, pp. 5–37, Springer Berlin Heidelberg, https://doi.org/10.1007/978-3-540-76619-3\_2.
- Golonka, J. (2004), Plate tectonic evolution of the southern margin of Eurasia in the Mesozoic and Cenozoic, *Tectonophysics*, 381(1–4), 235–73, https://doi.org/10.1016/j.tecto.2002.06.004.
- Gurbanov, G. H., I. I. Mardanov, and A. K. Gurbanov (2024), Characteristic of the scree formation process and influence on the development of floods in Nakchivan Autonomous Republic, *Journal of Geology, Geography and Geoecology*, 33(2), 263–273, https://doi.org/10.15421/112424.

- Herrmann, R. B. (1973), Some aspects of band-pass filtering of surface waves, *Bulletin of the Seismological Society of America*, 63(2), 663–671, https://doi.org/10.1785/bssa0630020663.
- Herrmann, R. B. (2013), Computer Programs in Seismology: An Evolving Tool for Instruction and Research, *Seismological Research Letters*, 84(6), 1081–1088, https://doi.org/10.1785/0220110096.
- Huang, Z., W. Su, Y. Peng, Y. Zheng, and H. Li (2003), Rayleigh wave tomography of China and adjacent regions, *Journal of Geophysical Research: Solid Earth*, 108(B2), https://doi.org/10.1029/2001JB001696.
- Ismail-Zadeh, A., S. Adamia, A. Chabukiani, et al. (2020), Geodynamics, seismicity, and seismic hazards of the Caucasus, *Earth-Science Reviews*, 207, 103,222, https://doi.org/10.1016/j.earscirev.2020.103222.
- Jackson, J., K. Priestley, M. Allen, and M. Berberian (2002), Active tectonics of the South Caspian Basin, *Geophysical Journal International*, 148(2), 214–245, https://doi.org/10.1046/j.1365-246x.2002.01588.x.
- Jrbashyan, R., G. Chlingaryan, Y. U. Kagramanov, et al. (2001), Geology of Meso-Cenozoic basins in Central Armenia, with comment on indications of hydrocarbons, *Search and Discovery Article* #30007.
- Karakhanian, A. S., V. G. Trifonov, H. Philip, et al. (2004), Active faulting and natural hazards in Armenia, eastern Turkey and northwestern Iran, *Tectonophysics*, 380(3–4), 189–219, https://doi.org/10.1016/j.tecto.2003.09.020.
- Keskin, M. (2003), Magma generation by slab steepening and breakoff beneath a subduction-accretion complex: An alternative model for collision-related volcanism in Eastern Anatolia, Turkey, *Geophysical Research Letters*, 30(24), https://doi.org/10.1029/2003GL018019.
- Khuduzade, A. I., and A. Jafarov (2017), Structural tectonic features of the south-eastern part of the Greater Caucasus the pre-Caspian GUBA as an example of the NQR, *Seismoprognosis Observations in the Territory of Azerbaijan*, 14(1).
- Klett, T. R. (2016), Geology and assessment of the undiscovered, technically recoverable petroleum resources of Armenia, 2013, US Geological Survey, https://doi.org/10.3133/ds69pp.
- Kornev, G. P. (1963), Minor intrusions and sills in the eastern Nakhichevan A.S.S.R. and the tectonics of their formations, *International Geology Review*, *5*(1), 28–37, https://doi.org/10.1080/00206816309474677.
- Koulakov, I., I. Zabelina, I. Amanatashvili, and V. Meskhia (2012), Nature of orogenesis and volcanism in the Caucasus region based on results of regional tomography, *Solid Earth*, 3(2), 327–37, https://doi.org/10.5194/sed-4-641-2012.
- Lebedev, V. A., I. V. Chernyshev, K. N. Shatagin, et al. (2013), The quaternary volcanic rocks of the Geghama highland, Lesser Caucasus, Armenia: Geochronology, isotopic Sr-Nd characteristics, and origin, *Journal of Volcanology and Seismology*, 7(3), 204–229, https://doi.org/10.1134/s0742046313030044.
- Legendre, C. P., T. L. Tseng, Y. N. Chen, et al. (2017), Complex deformation in the Caucasus region revealed by ambient noise seismic tomography, *Tectonophysics*, 712–713, 208–220, https://doi.org/10.1016/j.tecto.2017.05.024.
- Milyukov, V., E. Rogozhin, A. Gorbatikov, et al. (2018), Contemporary State of the Elbrus Volcanic Center (The Northern Caucasus), *Pure and Applied Geophysics*, 175(5), 1889–1907, https://doi.org/10.1007/s00024-017-1595-x.
- Mortezanejad, G., H. Rahimi, F. Romanelli, and G. F. Panza (2018), Lateral variation of crust and upper mantle structures in NW Iran derived from surface wave analysis, *Journal of Seismology*, 23(1), 77–108, https://doi.org/10.1007/s10950-018-9794-1.
- Pasyanos, M. E., W. R. Walter, and S. E. Hazler (2001), A Surface Wave Dispersion Study of the Middle East and North Africa for Monitoring the Comprehensive Nuclear-Test-Ban Treaty, in *Monitoring the Comprehensive Nuclear-Test-Ban Treaty: Surface Waves*, pp. 1445–1474, Birkhäuser Basel, https://doi.org/10.1007/978-3-0348-8264-4\_7.
- Perkins, S. (2019), Seismic tomography uses earthquake waves to probe the inner Earth, *Proceedings of the National Academy of Sciences*, 116(33), 16,159–16,161, https://doi.org/10.1073/pnas.1909777116.
- Rahimi, H. (2010), *Elastic and anelastic regional structures for crust and upper mantle in Iran (PhD thesis)*, International Institute of earthquake Engineering and seismology (IIEES).

- Raykova, R., and S. Nikolova (2007), Tomography and velocity structure of the crust and uppermost mantle in southeastern Europe obtained from surface wave analysis, *Studia Geophysica et Geodaetica*, 51(1), 165–184, https://doi.org/10.1007/s11200-007-0008-5.
- Ritzwoller, M. H., and A. L. Levshin (1998), Eurasian surface wave tomography: Group velocities, *Journal of Geophysical Research*: *Solid Earth*, 103(B3), 4839–4878, https://doi.org/10.1029/97JB02622.
- Ruppel, C., and M. McNutt (1990), Regional compensation of the Greater Caucasus mountains based on an analysis of Bouguer gravity data, *Earth and Planetary Science Letters*, 98(3–4), 360–379, https://doi.org/10.1016/0012-821x(90)9 0037-x.
- Skobeltsyn, G. A., R. Mellors, R. Gök, et al. (2014), Upper mantle S wave velocity structure of the East Anatolian-Caucasus region, *Tectonics*, 33(3), 207–221, https://doi.org/10.1002/2013TC003334.
- Sugden, P. J., I. P. Savov, M. Wilson, K. Meliksetian, G. Navasardyan, and R. Halama (2018), The Thickness of the Mantle Lithosphere and Collision-Related Volcanism in the Lesser Caucasus, *Journal of Petrology*, 60(2), 199–230, https://doi.org/10.1093/petrology/egy111.
- Sun, Y., M. N. Toksöz, R. J. Martin, et al. (2012), Crustal and uppermost mantle structure of Caucasus and surrounding regions, *Earthquake Science*, 25(5–6), 505–515, https://doi.org/10.1007/s11589-012-0874-y.
- Thybo, H. (2006), The heterogeneous upper mantle low velocity zone, *Tectonophysics*, 416(1–4), 53–79, https://doi.org/10.1016/j.tecto.2005.11.021.
- Trifonov, V. G., and V. I. Makarov (1988), Geologo-geomorphological study of modern tectonic movements, *Journal of Geodynamics*, 10(2–4), 309–320, https://doi.org/10.1016/0264-3707(88)90037-3.
- Tseng, T. L., H. C. Hsu, P. R. Jian, et al. (2016), Focal mechanisms and stress variations in the Caucasus and Northeast Turkey from constraints of regional waveforms, *Tectonophysics*, 691, 362–374, https://doi.org/10.1016/j.tecto.2016.10.028.
- Urban, L., A. Cichowicz, and F. Vaccari (1993), Computation of analytical partial derivatives of phase and group velocities for Rayleigh waves with respect to structural parameters, *Studia Geophysica et Geodaetica*, 37(1), 14–36, https://doi.org/10.1007/bf01613919.
- Wessel, P., and W. H. F. Smith (1995), New version of the generic mapping tools, *Eos, Transactions American Geophysical Union*, 76(33), 329–329, https://doi.org/10.1029/95EO00198.
- Yanovskaya, T. B. (1997), Resolution estimation in the problems of seismic ray tomography, *Izvestiya*, *Physics of the Solid Earth*, 33(9), 762–765.
- Yanovskaya, T. B., and P. G. Ditmar (1990), Smoothness criteria in surface wave tomography, *Geophysical Journal International*, 102(1), 63–72, https://doi.org/10.1111/j.1365-246x.1990.tb00530.x.
- Yanovskaya, T. B., E. S. Kizima, and L. M. Antonova (1998), Structure of the crust in the Black Sea and adjoining regions from surface wave data, *Journal of Seismology*, 2(4), 303–316, https://doi.org/10.1023/a:1009716017960.
- Zabelina, I., I. Koulakov, I. Amanatashvili, et al. (2016), Seismic structure of the crust and uppermost mantle beneath Caucasus based on regional earthquake tomography, *Journal of Asian Earth Sciences*, 119, 87–99, https://doi.org/10.1016/j.jseaes.2016.01.010.